

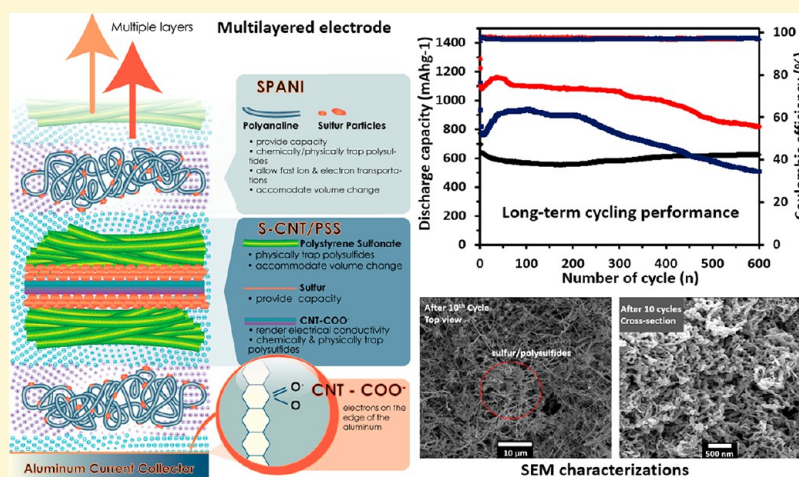
Long-Life, High-Efficiency Lithium–Sulfur Battery from a Nanoassembled Cathode

Jianhua Yan,^{†,‡} Xingbo Liu,[‡] Meng Yao,[‡] Xianfeng Wang,[†] Trina K. Wafle,[§] and Bingyun Li^{*,†,⊥}

[†]Biomaterials, Bioengineering, and Nanotechnology Laboratory; [‡]Department of Mechanical and Aerospace Engineering; and [§]National Research Center for Coal and Energy, West Virginia University, Morgantown, West Virginia 26506, United States

[⊥]National Energy Technology Laboratory, Regional University Alliance (NETL-RUA), Morgantown, West Virginia 26505, United States

Supporting Information



ABSTRACT: Lithium–sulfur (Li–S) batteries suffer from major problems including poor cycle performance and low efficiency, mainly due to the high solubility of intermediate polysulfides and their side-reactions with the Li-anode. Here, we report the development of advanced, multilayered, sulfur cathodes composed of alternately arranged, negatively charged S-carbon nanotube layers and positively charged S-polyaniline layers that effectively immobilize polysulfides and reduce polysulfide migration onto the Li-anode. The use of a layer-by-layer nanoassembly technique leads to a binder-free, three-dimensional porous cathode via electrostatic attraction and enables the fabrication of Li–S cells with remarkably improved performance including a long cycle life exceeding 600 cycles and a high Coulombic efficiency of 97.5% at the 1 C rate. Moreover, these Li–S cells have presented a high-rate response up to 2.5 C with high sulfur utilization (a reversible capacity of 1100 mAhg⁻¹, 900 mAhg⁻¹, 700 mAhg⁻¹, and 450 mAhg⁻¹ of sulfur at 0.3, 0.6, 1, and 2.5 C rates, respectively). The results provide important progress toward the understanding of the role of multilayered cathodes and the realization of high-efficiency and long-term service life for Li–S batteries.

Sulfur's high theoretical capacity of 1672 mAhg⁻¹, a 10-fold greater capacity versus today's lithium-ion batteries and sodium-ion batteries, makes lithium–sulfur (Li–S) batteries an attractive candidate to meet increasing demand for higher energy density energy storage devices.^{1–3} However, Li–S chemistry is inherently challenging.⁴ The formation of soluble, long-chain polysulfides (Li₂S_n, n ≥ 4) during discharge/charge cycling common to most present-day Li–S battery designs leads to the irreversible loss of active materials from the cathode into the electrolyte and onto the Li-anode. The polysulfides reduced at the anode cause a continuous evolution of porous Li metal structure thus leading to unstable solid-state electrolyte interface layers, damaging long-term cell performance, and presenting safety issues. Meanwhile, changes in the cathode morphology resulting from the volume change (80%) of sulfur during discharge/charge cycling induce strain inside

the cathode and cause the detachment of lithium polysulfides from the carbon surface, leading to low efficiency and fast capacity decay of cycling. Further, the chemistry results in uncontrollable deposition of Li₂S/Li₂S₂ species on both the cathode and anode surfaces, significantly inhibiting further lithiation, leading to low sulfur utilization.^{5–9}

Various sulfur–carbon composites and sulfur-conducting polymers have been used to realize high capacity and improve cycle life.^{10–15} Both approaches provide fast reactions and suppress the loss of soluble polysulfides during cycling. Other approaches focus on Li anode^{16,17} and electrolyte^{18,19} designs,

Received: May 13, 2015

Revised: June 30, 2015

Published: July 1, 2015

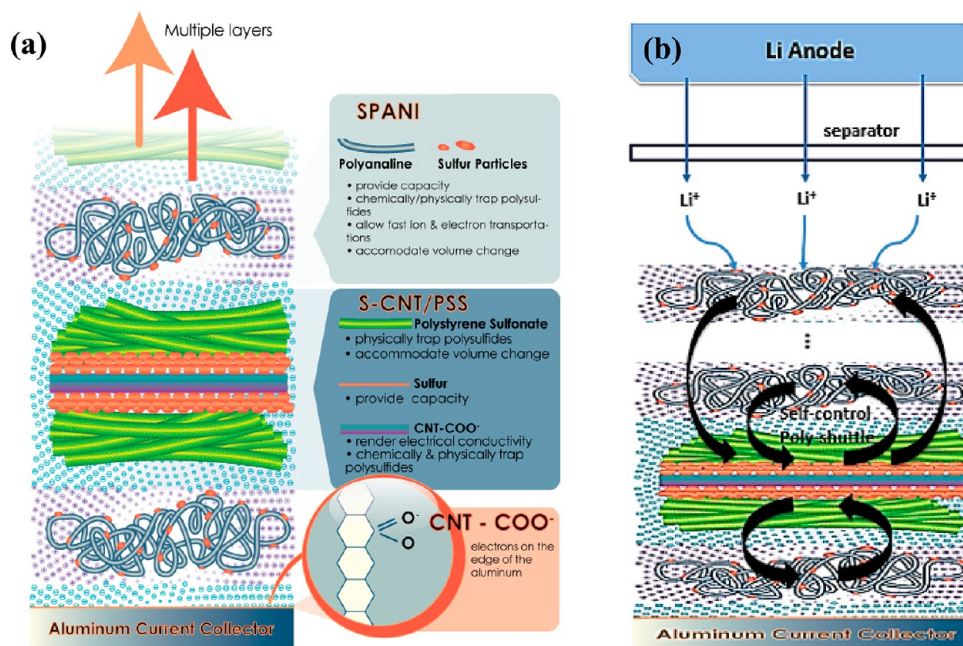


Figure 1. (a) Schematic diagram of multilayered cathode fabricated by the LbL nanoassembly process and functions of each component. (b) Schematic diagram of the self-control polyshuttle process in the multilayered cathode.

aiming to prevent undesirable interactions between polysulfides and the highly reductive Li-anode. However, these strategies can only slow the dissolution of polysulfides in the short term, and these approaches require significant use of binders, conductive agents, or modifying precursors in the cathode and thus neutralize the advantages of Li–S batteries. The detachment of highly polar polysulfides from nonpolar carbon conductive agents during discharge/charge and their subsequent dissolution into the electrolyte are still major concerns.^{11,12,20,21} Well-designed electrode structures and manipulation of sulfur distributions and attachments on the nanometer scale may be effective in enhancing the stability and performance of sulfur cathodes.

Here, we report the layer-by-layer (LbL)-nanoassembly²² fabrication of efficient, multilayered sulfur cathodes to address the challenges of Li–S batteries.²³ The multilayered cathodes were fabricated on aluminum current collectors by alternate adsorption of negatively charged S-carbon nanotubes polystyrenesulfonate (S-CNT-PSS⁻) and positively charged S-polyaniline nanotubes (SPANI)-NH⁺ as shown in Figure 1, panel a. Polyaniline (PANI) was deposited as the outermost layer to prevent direct contact between sulfur and the electrolyte. Both CNT^{24–28} and PANI^{29–31} are attractive choices as sulfur carriers because of their high electronic and ionic conductivities, strong affinity, and high loading of sulfur and polysulfides. The formed sandwich-like porous structures acted as self-control polyshuttle frameworks by forming physical and chemical barriers that reduced the migration of polysulfides from the cathode toward the Li-anode as shown in Figure 1, panel b. The developed multilayered cathodes were found to contain 67.5 wt % of sulfur, had high and stable reversible specific capacities of 1100, 900, and 700 mAhg⁻¹ at a current density of 0.3, 0.6, and 1 C, respectively, and provided a discharge/charge lifetime in excess of 600 cycles with an average Coulombic efficiency of 97.5%.

RESULTS AND DISCUSSION

Characterization of the Multilayered Cathodes and Related Materials.

Materials. S-CNT and SPANI were synthesized using functionalized CNT (FCNT) and PANI, respectively. The detailed synthetic procedures for these two materials are described in the Experimental Section. The pristine FCNT tended to agglomerate due to strong van der Waals interactions (Figure 2a). However, these interactions appeared to weaken after a thin layer of sulfur was coated on the surface of the FCNT (Figure 2b). The sulfur on the FCNT surface was evaluated by X-ray diffraction (XRD), in which obvious characteristic peaks of sulfur were observed for S-CNT (Figure S1a, Supporting Information). A monoclinic sulfur phase was detected by XRD in S-CNT after heating at 159 °C for 8 h and then 300 °C for 1.5 h. At 300 °C, elemental sulfur may react with FCNTs and form covalently bonded sulfur.^{26,32} C–S bonds formed were verified by the two additional peaks at 740 and 933 cm⁻¹ in the Fourier transform infrared spectroscopy (FTIR) analysis (Figure S1b) since it is known that S₈ shows no vibrational activity in the 900–2000 cm⁻¹ range.³³ The sulfur content in the S-CNT was found to be 76.9 wt % by thermogravimetric analysis (TGA) (Figure S1c). TGA results indicated that the weight loss and weight-loss temperature of S-CNT were higher than those of S/CNT composites, suggesting a promoted affinity and interaction between sulfur and FCNT.³⁴ The as-prepared PANI nanotubes were shown in Figure S2a. The typical morphology of the SPANI was shown in Figure 2, panel c where bulk sulfur particles were also found on SPANI surfaces, which may be attributed to strong capillary force during the postheat treatment. X-ray photoelectron spectroscopy (XPS) was conducted on the SPANI polymer, and the fitted curves indicated that the back-chains of PANI were chemically modified and physically coated with sulfur (Figures S2b–e). TGA results indicated that the sulfur content in SPANI was 65.4% (Figure S2f).

Multilayered Cathodes. The ultrahigh aspect ratio and good mechanical strength of FCNT and PANI led to a multilayered

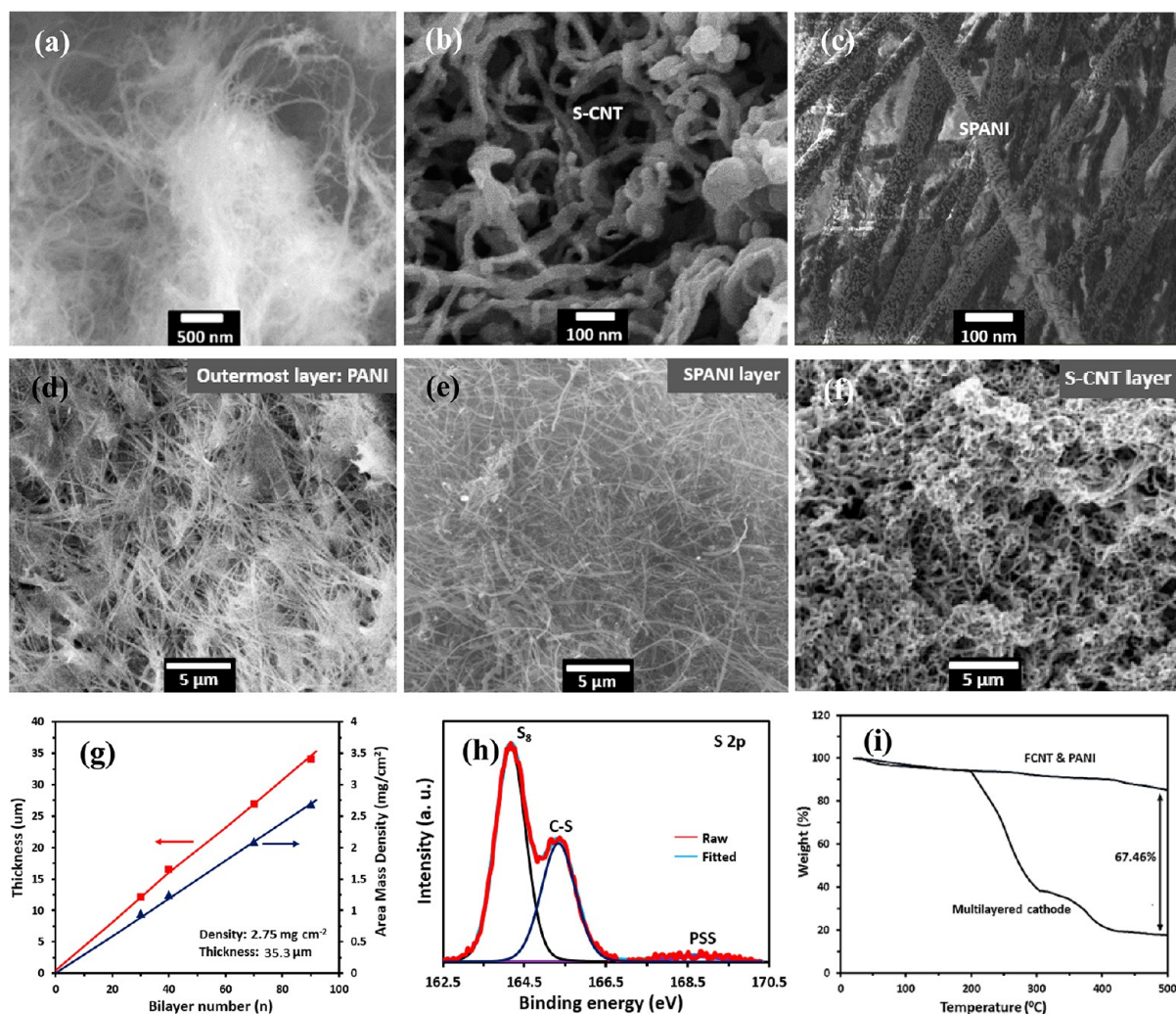


Figure 2. Characterizations of multilayered cathodes and related materials. (a–f) Scanning electron microscopy (SEM) images of (a) FCNT, (b) S-CNT, (c) SPANI, (d) the outermost layer, PANI, (e) SPANI layer, and (f) S-CNT layer. (g) Area mass density (mg cm^{-2}) and thickness (μm) versus bilayers of multilayered cathodes on aluminum current collectors. (h) XPS and (i) TGA analysis of the multilayered cathodes. In panel i, the sample of FCNT and PANI was used as a background comparison for the calculation of sulfur content in the multilayered cathodes. The sample was prepared with the same method for fabricating the multilayered SCNT–SPANI cathodes.

cathode with a robust structure that possessed abundant interconnected channels through which Li ions might pass (Figure 2d–f). These channels formed three-dimensional (3-D) porous frameworks that favored the penetration of electrolytes. Since sulfur is involved in multistep reactions during discharge and charge, Li-ion and electron transports are important factors. The empty pores in the multilayered cathode acted as reservoirs for liquid electrolytes capable of fast Li-ion conduction. Meanwhile, the highly intertwined PANI and FCNT facilitated electrical conductivity and, to a lesser extent, Li-ion transport. The multilayered structure formed a 3-D integrated skeleton, and the discrete layers ensured a homogeneous sulfur distribution. The skeleton provided large reactive interfacial areas that allowed easy incorporation and manipulation of sulfur. The structure facilitated electronic and ionic conduction across the multilayered interfaces between the discrete layers and the electrolyte, maximizing the efficiency of sulfur in combining with lithium. The thickness of the multilayered cathode increased approximately linearly with the increasing number of bilayers; the cathode with 90 bilayers had a thickness of $35.3 \mu\text{m}$ with a total material density of 2.75

mg cm^{-2} after heat treatment (Figure 2g). XPS analysis of the multilayered cathodes after heat treatment revealed significant amounts of S₈ and C–S bonds within the cathodes (Figure 2h). The peak at 164.4 eV in the S 2p_{3/2} spectrum indicated elemental sulfur, while the peak at 165.4 eV in the S 2p_{1/2} spectrum suggested that S atoms were linked to a benzenoid ring (SPANI) and a quinoid ring (sulfurized CNT). The small peak at 168.5 eV corresponded to PSS. The atomic composition of the multilayered cathode was found to be 29.2 wt % carbon, 64.1 wt % sulfur, 4.6 wt % oxygen, and 2.1 wt % nitrogen. TGA results indicated that the sulfur content in the whole cathode was 67.5%, corresponding to a sulfur loading of 1.85 mg cm^{-2} (Figure 2i).

Electrochemical Performance of Multilayered Cathodes. The rate capability of multilayered cathodes is shown in Figure 3, panel a. The C rates specified in this study are based on the theoretical capacity of sulfur, with $1 \text{ C} = 1675 \text{ mA g}^{-1}$. Since the sulfur loading of multilayered cathode was 1.85 mg cm^{-2} , the C rate could be calculated by $1 \text{ C} = 3.1 \text{ mA cm}^{-2}$. The initial discharge capacity reached 1346 mAh g^{-1} of sulfur at 0.1 C , which is 80.4% of the theoretical value for sulfur. A reversible

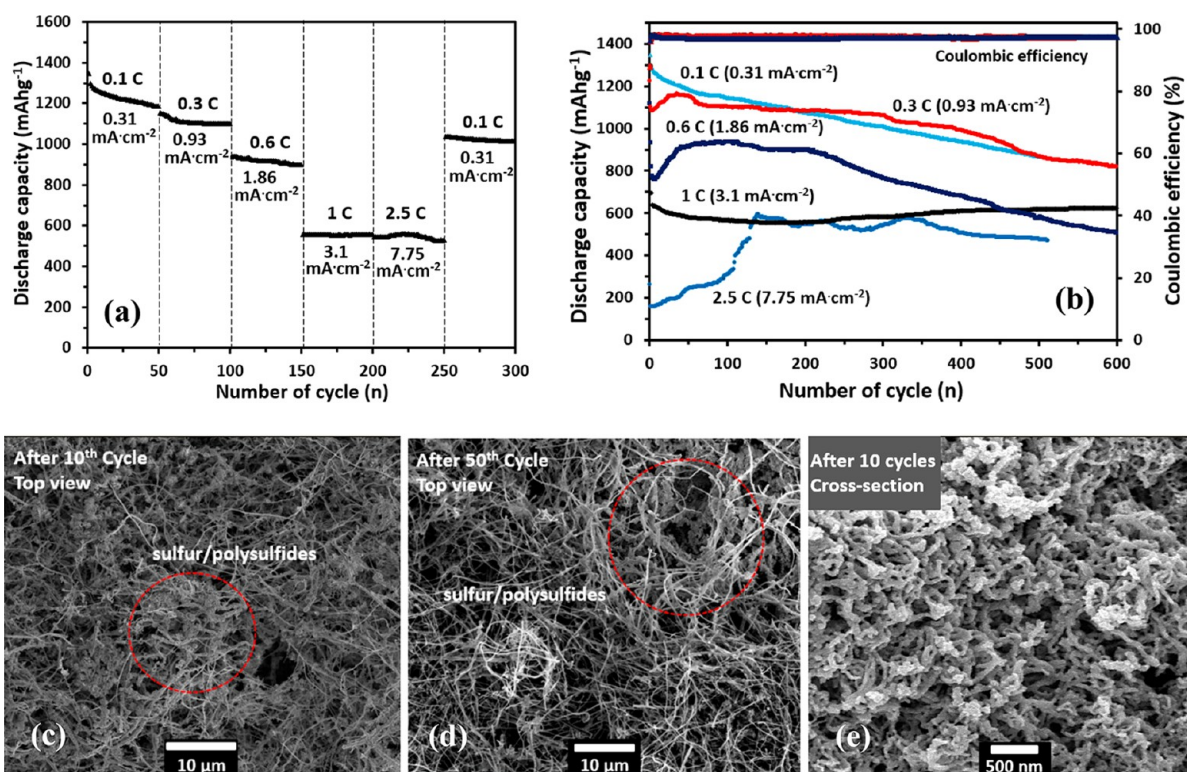


Figure 3. Electrochemical performance of Li–S cells employing multilayered cathodes and SEM characterizations of the cathodes at different cycles. (a) Rate performance and (b) long-term cycling performance of multilayered cathodes at different current rates. (c) Top view and (e) cross-section at the 10th cycle, and (d) top view at the 50th cycle of multilayered cathodes.

capacity of 1014 mAhg^{-1} was observed at the 300th cycle, corresponding to 75.3% capacity retention. The results demonstrated the superiority of the multilayered structure in enhancing the active material utilization. As current density varied from 0.1 to 2.5 C, the multilayered cathodes still displayed reasonable capacity, although capacity decreased gradually, which may be due to the polarization effect. Even at a rate of 2.5 C, the cell capacity exceeded 580 mAhg^{-1} after 150 cycles, demonstrating high rate performance and robust structure.

The long-term cycling behavior and Coulombic efficiency of Li–S cells containing multilayered cathodes at different current densities are shown in Figure 3, panel b. Significantly improved cycling stability was observed at the current densities studied. For instance, at 0.3 C, the multilayered cathodes had a high reversible capacity of 1100 mAhg^{-1} . A reversible capacity of 818 mAhg^{-1} was obtained even after 600 cycles, corresponding to 74.4% of capacity retention with an average Coulombic efficiency of 97.5%. It is noteworthy to mention that Li–S cells using the same multilayered cathode but having no lithium nitrate additive in electrolyte also had a high Coulombic efficiency of 96.3% (Figure S3), while the traditional Li–S cells using slurry-coating sulfur cathodes had a much lower Coulombic efficiency of $\sim 80\%$ (Figure S4). These results indicated that the polysulfide shuttling effects were significantly mitigated in the multilayered sulfur cathode based cells. Unlike traditional sulfur cathodes with poor contact between sulfur and carbon during discharge/charge, the multilayered sulfur structure provided strong affinity of polysulfides/sulfur and reduced their dissociation from the interconnected network of CNTs and PANIs during cycling (Figure 3c,d). The intimate contact layers within the multilayered structure further attracted

polysulfide anions and prevented the anions from “leaking” out (Figure 3e). In addition, the porous frameworks in the multilayered cathodes accommodated the volume change of the sulfur and the corresponding strains accumulated in the cathodes, thus leading to improved cycling stability.

The current density also had a great influence on the discharge reactions (Figure 3b). At a high current density of 2.5 C, the discharge capacity of multilayered cathodes reached a steady state after 130 cycles, probably because sulfur could not be reacted until it was exposed to the electrolyte after the initial cycles at high C rates.³⁵ However, at a low current density of 0.1 C, we estimated that $\sim 80\%$ of sulfur reacted with lithium from the beginning of the test. However, at moderate current densities of 0.3, 0.6, and 1 C, a decrease in the first few cycles followed by an increase in discharge capacity was observed (Figure 3b). The decrease was probably caused by the catalytic reduction of electrolyte solvents on the fresh surfaces of the multilayers and the formation of solid electrolyte interface films on Li-anodes. The increase was probably related to the high solubility of polysulfides in electrolytes.⁸ Initially, the cathodes contained bulk sulfur, which could not completely react at the end of discharge. After a few cycles, the electrolyte infiltrated into the internal layers, and the bulk sulfur reacted and pulverized, leading to small sulfur particles. Subsequently, the cells reached a steady state and showed stable cyclic properties. Particularly, it took a longer time for the battery at 1 C to reach the steady state; the intrinsic mechanism controlling this phenomenon is still under investigation.

Electrochemical Reaction Processes in Multilayered Cathodes. The electrochemical reaction mechanism of sulfur in multilayered cathodes was revealed using cyclic voltammetry (CV) at a scan rate of 0.05 mV s^{-1} . As shown in Figure 4, panel

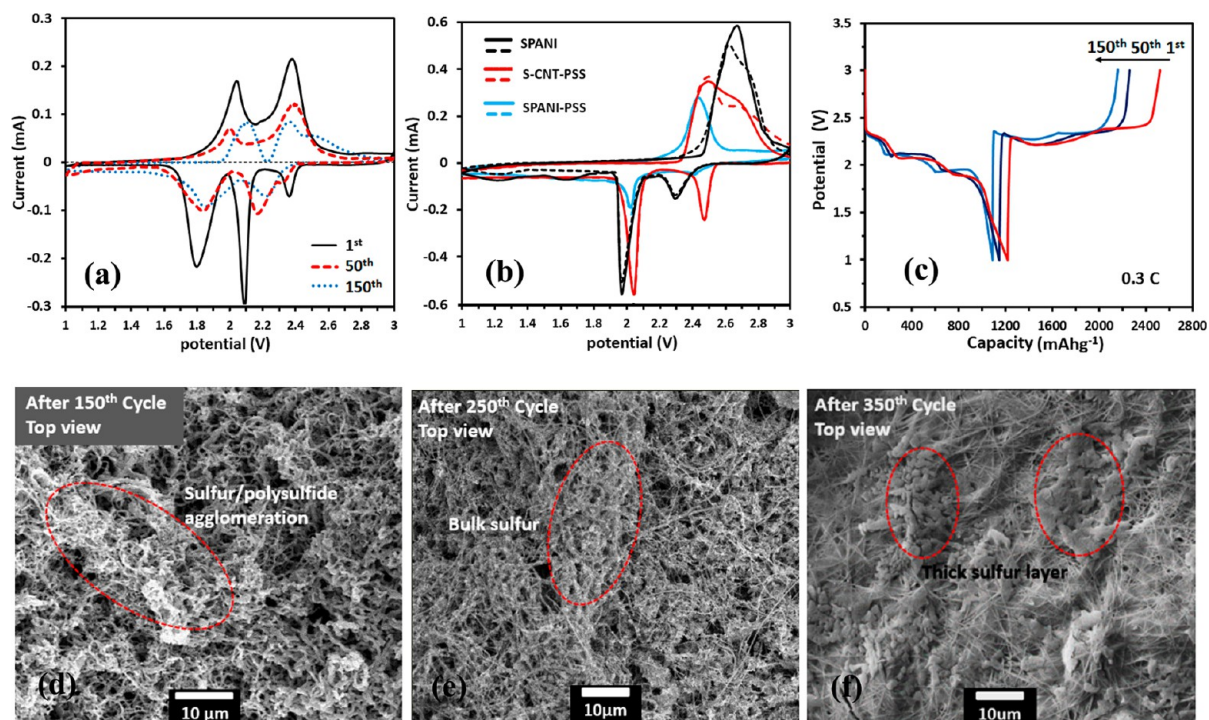


Figure 4. Electrochemical performance of Li–S cells employing multilayered cathodes and SEM characterizations of the cathodes at different cycles. (a) CV scans of multilayered cathodes (scan rate was 0.05 mV s^{-1}). (b) CV scans of SPANI, SPANI-PSS, and S-CNT-PSS based cathodes. The scan rate was 0.05 mV s^{-1} . The SPANI cathodes contained 10 wt % of PVDF and 90 wt % of SPANI; the SPANI-PSS (S-CNT-PSS) cathodes contained 10 wt % of PVDF, 30 wt % of PSS, and 60 wt % of SPANI (S-CNT). The solid line indicates the first cycle, and the dotted line indicates the second cycle of the CV tests. (c) Voltage profiles of multilayered cathodes at 1st, 50th, and 150th cycles. Top surface characterization of multilayered cathodes at (d) 150th, (e) 250th, and (f) 350th cycles.

a, the fresh multilayered cathode featured three reduction current peaks at around 2.38, 2.1, and 1.8 V. The first two narrow peaks showed typical characteristics of two-step reduction of sulfur from solid–liquid (S_8 – S_6^{2-}) and liquid–solid (S_6^{2-} – Li_2S_2) phase transitions. The third broad reduction current peak at 1.8 V was lower than the potential of S_4^{2-} to Li_2S_2 reaction at around 2.1 V. Similarly, multilayered cathodes without lithium nitrate additives had three reduction peaks (Figure S5). However, SPANI, SPANI-PSS, and S-CNT-PSS based cathodes presented typical sulfur characteristics with two reduction peaks at 2.30 and 1.97, 2.31 and 2.01, and 2.44 and 2.04 V, respectively (Figure 4b). These observations indicated that the multilayered cathodes experienced a new reaction represented by the reduction peak at 1.8 V, which was possibly attributed to the reaction from Li_2S_2 to Li_2S . As shown in Figure S6, the four characteristic peaks at 23° , 31° , 45° , and 50° in the XRD pattern indicated the existence of Li_2S . However, the CV curves at the 50th cycle showed significantly different behavior. The first two reduction peaks shown in the initial cycle were substituted by a new broad peak centered at 2.2 V in the 50th cycle. Most likely, the high potential polarization between soluble, high-order polysulfides (HPS, i.e., Li_2S_n , $n \geq 3$) and insoluble, low-order polysulfides (Li_2S_n , $n \leq 2$) caused an overlap of the two possible reduction peaks. The continuous CV scan of the multilayered cathodes shown in Figure S7 demonstrated gradual changes during the electrochemical reaction processes.

At 0.3 C, the discharge/charge profiles of multilayered cathodes in Figure 4, panel c exhibited three discharge plateaus at 2.3, 2.1, and 1.9 V and two discrete charge plateaus at 2.3 and 2.4 V, which were consistent with the CV analyses. Similar

results were observed at 0.6 and 1.0 C (Figure S8). The upper discharge plateau at 2.3 V corresponded to the reduction of sulfur into soluble lithium polysulfides. The discharge capacity values of the cell corresponding to this plateau at the first, 50th, and 150th cycles were identical, demonstrating the effectiveness of the multilayered cathode in trapping soluble polysulfides and enhancing the utilization of sulfur. When sulfur in each layer is reduced upon full discharge, the strong affinity of polysulfides for the sandwich-like porous frameworks is vital for retaining the active mass and electrical contact of sulfur/polysulfides within the conductive framework. SEM images (Figure 4d–f) of the multilayered cathodes in the discharged state revealed that the discharge products were kept within the cathode structure to form thick layers instead of discrete particles, implying the strong interaction between polysulfides and the multilayered structure. The thick sulfur layer observed on the surface of the cathode could be attributed to the insoluble Li_2S or Li_2S_2 layers formed at the end of discharge.

The multilayered sulfur cathodes reduced the dissolution of polysulfides probably because, in the multilayered structure design, the alternately arranged SPANI layers and S-CNT-PSS layers not only provided capacity, but also served as chemical and physical barriers that reduced unwanted polysulfide migration from the cathode to the electrolyte. The electrostatic interaction between the alkylammonium cations and polysulfide anions might also trap polysulfides during the repeated cycles,^{12,28} leading to high cycling stability. In addition, multiple studies have shown that chemical interactions between sulfur or polysulfide with an oxygen functional group, nitrogen group, or unsaturated carbon bonds on CNT and PANI in the multilayered cathodes could reduce the dissolution of

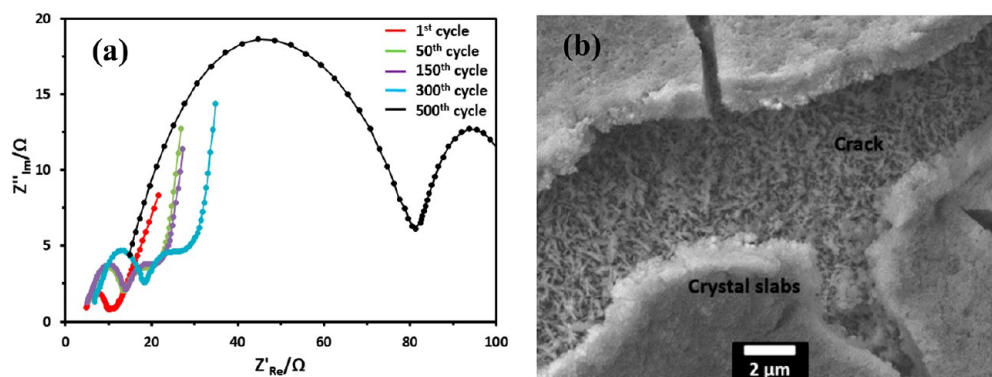


Figure 5. EIS analysis of the Li–S cells containing multilayered cathodes. (a) EIS analysis of Li–S cells with multilayered cathodes. (b) SEM image of cathode surface after 500 cycles.

polysulfides.^{36–40} The porous 3-D framework in the multilayered structure provided efficient electron and Li-ion conduction, which contributed to a high utilization of sulfur and fast kinetics.

Electrochemical impedance spectra (EIS) analysis was performed to further evaluate the multilayered cathodes. As shown in Figure 5, panel a, the EIS spectra were composed of two semicircles at the high frequency region and an inclined tail in the low frequency region. The real axis intercepting at the high frequency represented the electrolyte resistance. The semicircle from high to medium frequency corresponded to the solid-electrolyte interface (SEI) layer resistance, and the second semicircle at medium frequency was related to the charge-transfer resistance. The short inclined line in the low frequency regions was due to ionic diffusion within the cathode. The interfacial charge-transfer resistance was recognizable from the second semicircle owing to the redox formation of soluble polysulfides and insoluble short-chain polysulfides. The resistances at the 50th and 150th cycles were identical, indicating a stable SEI layer on the lithium surface and a smooth charge transfer of lithium ions in the cell. These findings might indicate that there was limited polysulfide shuttling in the first 150 cycles since otherwise, the dissolved polysulfides would migrate toward the Li-anode, at which point they would be reduced to low order polysulfides (LPS) and irreversibly precipitate onto the Li-anode surface. This would inhibit charge transfer of lithium ions thereby leading to an increase in cell impedance. Cathode kinetics and charge-transfer polarization accounted for the majority of the voltage loss in the cells. The multilayered cathodes had low resistance, which presented an ideal opportunity to create intimate organic–inorganic interfaces for efficient electrochemical reactions in Li–S batteries. At the 500th cycle, by contrast, both the interfacial resistance and charge-transfer resistance increased. The reactions of sulfur resulted in great morphological changes at the 500th cycle, leading to (i) obvious cracks and (ii) formation of crystal slabs on the surfaces of the multilayered cathodes (Figure 5b). Both the nonconductive crystal slabs and the cracks caused high resistance within the cell.

CONCLUSION

In this work, we demonstrated a unique multilayered sulfur electrode fabricated with LbL nanoassembly method. With this method, extra cell components such as PVDF binders were not necessary. Within the multilayered structure, the intercon-

nected PANI and FCNT layers served as an electrical conductive network, and the abundance of pores served as ionic conductive pathways. The CNTs and PANIs could physically separate sulfur layers and maintain a high surface area, and led to enhanced sulfur utilization. The discharge/charge voltage profiles and the CV scans, combined with the EIS, XPS, and FTIR analyses, revealed that the multilayered cathodes resulted in reduced polysulfide shuffling effects and more complete sulfur transformation, leading to excellent cell operation with high efficiency, good reversibility, and fast kinetics. SEM images showed no significant structural damage to the multilayered cathode before 350 cycles, indicating high structural stability of the multilayered cathode. As a result, the multilayered cathodes provided a long lifetime of more than 600 cycles with an average Coulombic efficiency of 97.5% under a variety of discharge/charge current densities. The tunable nature of the LbL technique allows for the incorporation and manipulation of nonconductive sulfur and highly conductive CNTs/PANIs. These multilayered cathodes may contribute to potential development and applications of long-lived, high energy density, and high power Li–S batteries for electric vehicle systems and flexible and thin-film devices.

EXPERIMENTAL SECTION

Chemicals. Multiwalled carbon nanotubes (110–170 nm in diameter and 5–9 μm in length), nitric acid (70 wt %), sulfuric acid (95–98 wt %), sodium dodecyl sulfate (SDS) solution (20% in water), sulfur powder (99.998%), tetrahydrofuran (99.9%, THF), aniline (99.5%), sodium dodecylbenzenesulfonate (SDBS), ammonium persulfate (98%), sulfur monochloride (98%), aluminum chloride (99.99%), sodium sulfide, N,N-dimethylformamide (99.8%, DMF), NH_2OH solution (50% in water), carbon disulfide solution (99%, CS_2), and poly(styrenesulfonate) (PSS, MW $\sim 70,000$) were purchased from Sigma-Aldrich, Co. LLC, United States.

Materials Preparation. *Preparation of S-CNT Composites.* Multiwalled carbon nanotubes (800 mg) were soaked in nitric acid and sulfuric acid (60 mL, v 1:3) in an ultrasonic container for 1 h, kept in an oven of 70 $^\circ\text{C}$ for 2 h, and then rinsed six times with distilled water to get FCNTs. The FCNTs (~ 100 mg) were dispersed into SDS aqueous solution (15 mL). Meanwhile, sulfur powder (500 mg) was dissolved in THF (15 mL) to form a saturated solution. Next, the sulfur-saturated THF and FCNTs in SDS were mixed for 12 h under magnetic stirring, then centrifuged. The supernatant was decanted, and the remaining materials were washed using deionized water to remove SDS. Finally, the as-prepared S-CNTs were mixed with sulfur (1:1 wt %) and treated in a vacuum oven at 159 $^\circ\text{C}$ for 8 h and then at 300 $^\circ\text{C}$ for 1.5 h.

Preparation of SPANI. Aniline, SDBS, and ammonium persulfate (M 1:1:1) were dissolved in hydrochloride aqueous solution for 40 h,

washed using distilled water, and dried in a vacuum oven at room temperature for 24 h to obtain PANI nanotubes. PANI, sulfur monochloride, and aluminum chloride (M 1:1:2) were soaked in acetonitrile in a sealed flask for 10 h, washed using ether, and dried in a vacuum oven at 80 °C for 24 h to obtain chloride PANI. Sulfur and sodium sulfide (M 4:1) were then mixed in DMF (10 mL) in a vacuum oven for 6 h to obtain disodium pentasulfide (Na_2S_5). Next, the chloride PANI was soaked in a Na_2S_5 solution for 24 h in a vacuum oven, washed with deionized water, and dried in a vacuum oven at 80 °C for 24 h to achieve initial sulfurized PANI. Finally, the initial sulfurized PANI was mixed with sulfur (1:1 wt %) in carbon disulfide solution (CS_2) for 2 h under magnetic stirring and heated in a vacuum oven at 280 °C for 2 h to obtain SPANI.

Fabrication of Multilayered Cathodes Using LbL Nano-assembly Technique. *Aluminum Substrate Treatment.* Aluminum current collector was used as the substrate for the LbL process, and a thin layer of CNT-COO⁻ was deposited on the substrate by electrophoretic deposition (EPD) technique.

LbL Process. First, SPANI was treated with NH_2OH solution at 70 °C for 2 h, and S-CNT was mixed with PSS solution for 2 h. These treated powders were then sonicated for 6 h in deionized water separately. The pH values of both solutions were adjusted to 3.5, and the solutions were sonicated for 3 h before LbL assembly. The purpose of introducing PSS here was to facilitate the growth of the multilayer films via electrostatic interactions; PSS is a strong polyelectrolyte. Details of LbL assembly of cathodes can be found elsewhere.^{41–44} In brief, the process involves immersing the treated substrate into the SPANI suspension for 3 min and then washing the substrate in deionized water for 30 s and next, placing the SPANI-coated substrate into S-CNT suspension for 3 min and then washing in deionized water for 30 s. These steps are repeated until the desired number of layers is achieved. In the present study, the multilayered cathode has 90 bilayers with sulfur loading of 1.85 mg cm^{-2} . Finally, the assembled multilayered cathodes are dried in air and treated at 100 °C in a vacuum oven for 5 h. The cathode is now ready to be assembled into a cell. Note that the LbL method can produce a large number of samples by robot machines and has the potential for large-scale industrial applications.⁴⁵

XPS, XRD, and FTIR Measurements. Kratos Axis Ultra XPS (Kratos Analytical) with a monochromatized Al K α X-ray source, PANalytical XRD, and FTS 7000 FTIR were used to analyze the surface chemistry of S-CNT, SPANI, and multilayered cathodes. Curve fittings of the XPS spectra were performed following a Shirley-type background subtraction.

Electrochemical Measurements of Multilayered Cathode-Based Cells. CR2016-type coin cells were used as the testing cells. Lithium foils were used as the anodes, Cellgard 2400 microporous membranes as separators, 1.0 mol L^{-1} bis(trifluoromethane sulfonyl) imide (LiTFSI) and 0.15 mol L^{-1} LiNO_3 dissolved in dioxolane (DOL) and dimethoxyethane (DME) (1:1, v/v) as electrolytes, and S-CNT/SPANI multilayered composite as cathodes. The cells were assembled in an argon-filled glovebox. Electrochemical measurements were performed galvanostatically between 1.0 and 3.0 V at current densities of 550, 1300, 1950, and 6400 mA g^{-1} . Capacity was calculated based on the weight of all materials on the cathodes. CV experiments were conducted using a NOVA potentiostat at scan rates of 5, 0.5, and 0.1 mVs^{-1} . EIS measurements were carried out using a NOVA electrochemical workstation in a frequency range between 100 kHz and 100 mHz at a potentiostatic signal amplitude of 5 mV. All experiments were conducted at room temperature.

■ ASSOCIATED CONTENT

● Supporting Information

XRD analysis of S-CNT, SPANI, and FCNT. FTIR spectra of S-CNT and FCNT. TGA and DSC analysis of S-CNT showing 76.9 wt.% of sulfur in the S-CNT composite. SEM image of PANI nanotubes fabricated in this study. Wide range XPS spectra of PANI and the obtained SPANI. XPS data of S 2p, C 1s, and N 1s regions of SPANI. TGA and DSC analysis of

SPANI showing 65.4 wt.% of sulfur in SPANI composite. Coulombic efficiency and long-term cycling performance of multilayered cathodes without lithium nitrate additive. Cycling performance at various current densities for the slurry-coated cathodes that contained 10 wt % of PVDF, 45 wt % S-CNT, and 45 wt % SPANI. CV data of Li–S cells employing multilayered cathodes and electrolyte without lithium nitrate additives. XRD data of the multilayered cathode after the 50th discharge. Continuous CV scans of multilayered cathodes for the first three cycles. Initial voltage profiles of multilayered cathodes. The Supporting Information is available free of charge on the ACS Publications website at DOI: 10.1021/acs.chemmater.5b01780.

■ AUTHOR INFORMATION

Corresponding Author

*E-mail: bili@hsc.wvu.edu.

Author Contributions

J.Y. and B.L. conceived and designed the experiments. J.Y. conducted the multilayered film assembly and carried out characterization analysis for the cathodes and Li–S cells. M.Y. helped with the EPD experiments. X.W. helped with the SEM tests. X.L. and B.L. supervised the work and were involved in the discussions. T.W. helped with the schematic diagrams. J.Y. wrote the manuscript. Technical editing was provided by B.L. and T.W. All authors reviewed and approved the final manuscript.

Notes

The authors declare no competing financial interest.

■ ACKNOWLEDGMENTS

This work was funded by a Research Challenge Grant of the West Virginia Higher Education Policy Commission Division of Science and Research. The authors acknowledge use of the West Virginia University (WVU) Shared Research Facilities and financial support from West Virginia Higher Education Policy Commission Division of Science and Research. We appreciate the assistance of Weiqiang Ding, Ph.D., in collecting XPS, XRD, and FTIR data and Marcela Redigolo, Ph.D., in collecting SEM and EDS figures. We thank Jie Xiao, Ph.D., for discussions.

■ REFERENCES

- (1) Dunn, B.; Kamath, H.; Tarascon, J. M. Electrical Energy Storage for the Grid: A Battery of Choices. *Science* **2011**, *334*, 928–934.
- (2) Yan, J.; Liu, X.; Li, B. Recent Progress in Li-Rich Layered Oxides as Cathode Materials for Li-ion Batteries. *RSC Adv.* **2014**, *4*, 63268–63284.
- (3) Yan, J.; Liu, X.; Li, B. Nano-Assembled $\text{Na}_2\text{FePO}_4\text{F}$ /Carbon Nanotube Multi-Layered Cathodes for Na-Ion Batteries. *Electrochem. Commun.* **2015**, *56*, 46–50.
- (4) Bruce, P. G.; Freunberger, S. A.; Hardwick, L. J.; Tarascon, J. M. Li-O₂ and Li-S Batteries with High Energy Storage. *Nat. Mater.* **2011**, *11*, 19–29.
- (5) Yang, Y.; Zheng, G. Y.; Cui, Y. Nanostructured Sulfur Cathodes. *Chem. Soc. Rev.* **2013**, *42*, 3018–3032.
- (6) Whittingham, M. S. Lithium Batteries and Cathode Materials. *Chem. Rev.* **2004**, *104*, 4271–4302.
- (7) Ellis, B. L.; Lee, K. T.; Nazar, L. F. Positive Electrode Materials for Li-ion and Li-batteries. *Chem. Mater.* **2010**, *22*, 691–714.
- (8) Zhang, S. S. Liquid Electrolyte Lithium/Sulfur Battery: Fundamental Chemistry, Problems, and Solutions. *J. Power Sources* **2013**, *231*, 153–162.

- (9) Zhang, S. S. New Insight into Liquid Electrolyte of Rechargeable Lithium/Sulfur Battery. *Electrochim. Acta* **2013**, *97*, 226–230.
- (10) Tang, C.; Zhang, Q.; Zhao, M.; Huang, J.; Cheng, X.; Tian, L.; Peng, H.; Wei, F. Nitrogen-doped Aligned Carbon Nanotube/Graphene Sandwiches: Facile Catalytic Growth on Bifunctional Natural Catalysts and Their Applications as Scaffolds for High-rate Lithium-Sulfur Batteries. *Adv. Mater.* **2014**, *26*, 6100–6105.
- (11) Zheng, G.; Zhang, Q.; Cha, J. J.; Yang, Y.; Li, W.; Seh, Z. W.; Cui, Y. Amphiphilic Surface Modification of Hollow Carbon Nanofibers for Improved Cycle Life of Lithium Sulfur Batteries. *Nano Lett.* **2013**, *13*, 1265–1270.
- (12) Wang, Z.; Dong, Y.; Li, H.; Zhao, Z.; Bin Wu, H.; Hao, C.; Liu, S.; Qiu, J.; Lou, X. Enhancing Lithium-Sulphur Battery Performance by Strongly Binding the Discharge Products on Amino-Functionalized Reduced Graphene Oxide. *Nat. Commun.* **2014**, *5*, 5002.
- (13) Su, Y.; Manthiram, A. Lithium-Sulphur Batteries with a Microporous Carbon Paper as a Bifunctional Interlayer. *Nat. Commun.* **2012**, *3*, 1166.
- (14) Wang, H.; Yang, Y.; Liang, Y.; Robinson, J. T.; Li, Y.; Jackson, A.; Cui, Y.; Dai, H. Graphene-Wrapped Sulfur Particles As A Rechargeable Lithium-Sulfur Battery Cathode with High Capacity and Cycling Stability. *Nano Lett.* **2011**, *11*, 2644–2647.
- (15) Yan, J.; Liu, X.; Wang, X.; Li, B. Long-life, High-Efficiency Lithium/Sulfur Batteries from Sulfurized Carbon Nanotube Cathodes. *J. Mater. Chem. A* **2015**, *3*, 10127–10133.
- (16) Huang, C.; Xiao, J.; Shao, Y.; Zheng, J.; Bennett, W.; Lu, D.; Laxmikant, S. V.; Engelhard, M.; Ji, L.; Zhang, J.; et al. Manipulating Surface Reactions in Lithium-Sulphur Batteries Using Hybrid Anode Structures. *Nat. Commun.* **2014**, *5*, 3015.
- (17) Zheng, G.; Lee, S. W.; Liang, Z.; Lee, H.; Yan, K.; Yao, H.; Wang, H.; Li, W.; Chu, S.; Cui, Y. Interconnected Hollow Carbon Nanospheres for Stable Lithium Metal Anodes. *Nat. Nanotechnol.* **2014**, *9*, 618–623.
- (18) Suo, L.; Hu, Y.; Li, H.; Armand, M.; Chen, L. A New Class of Solvent-in-Salt Electrolyte for High-Energy Rechargeable Metallic Lithium Batteries. *Nat. Commun.* **2013**, *4*, 1481.
- (19) Aurbach, D.; Pollak, E.; Elazari, R.; Salitra, G.; Kelley, C. S.; Affinito, J. On the Surface Chemical Aspects of Very High Energy Density, Rechargeable Li-Sulfur Batteries. *J. Electrochem. Soc.* **2009**, *156*, A694–A702.
- (20) Elazari, R.; Salitra, G.; Talyosef, Y.; Grinblat, J.; Scordilis-Kelley, C.; Xiao, A.; Affinito, J.; Aurbach, D. Morphological and Structural Studies of Composite Sulfur Electrodes Upon Cycling by HRTEM, AFM and Raman Spectroscopy. *J. Electrochem. Soc.* **2010**, *157*, A1131–1138.
- (21) Nelson, J.; Misra, S.; Yang, Y.; Jackson, A.; Liu, Y.; Wang, H.; Dai, H.; Andrews, J. C.; Cui, Y.; Toney, M. F. In Operando X-ray Diffraction and Transmission X-ray Microscopy of Lithium Sulfur Batteries. *J. Am. Chem. Soc.* **2012**, *134*, 6337–6343.
- (22) Decher, G. Fuzzy Nanoassemblies: Toward Layered Polymeric Multicomposites. *Science* **1997**, *277*, 1232–1237.
- (23) Yan, J.; Liu, X.; Li, B. Development of Lithium Sulfur Batteries with Improved Cycle Life and High-Power Properties. *ECS Meet. Abstr.* **2014**, 186.
- (24) De Volder, M. F. L.; Tawfik, S. H.; Baughman, R. H.; Hart, A. J. Carbon Nanotubes: Present and Future Commercial Applications. *Science* **2013**, *339*, 535–539.
- (25) Yan, J.; Liu, X.; Li, B. Innovative Sulfur-Carbon Nanotube Cathodes for High-Performance Li/S Batteries. *ECS Meet. Abstr.* **2015**, 290.
- (26) Guo, J.; Xu, Y.; Wang, C. Sulfur-Impregnated Disordered Carbon Nanotubes Cathode for Lithium-Sulfur Batteries. *Nano Lett.* **2011**, *11*, 4288–4294.
- (27) Jia-Jia, C.; Xin, J.; Qiu-Jie, S.; Chong, W.; Qian, Z.; Ming-Sen, Z.; Quan-Feng, D. The Preparation of Nano-Sulfur/MWCNTs and Its Electrochemical Performance. *Electrochim. Acta* **2010**, *55*, 8062–8066.
- (28) Xu, T.; Song, J. X.; Gordin, M. L.; Sohn, H. S.; Yu, Z. X.; Chen, S. R.; Wang, D. H. Mesoporous Carbon-Carbon Nanotube-Sulfur Composite Microspheres for High-Areal-Capacity Lithium-Sulfur Battery Cathodes. *ACS Appl. Mater. Interfaces* **2013**, *5*, 11355–11362.
- (29) Xiao, L.; Cao, Y.; Xiao, J.; Schwenzler, B.; Engelhard, M. H.; Saraf, L.; Nie, Z.; Exarhos, G. J.; Liu, J. A Soft Approach to Encapsulate Sulfur: Polyaniline Nanotubes for Lithium-Sulfur Batteries with Long Cycle Life. *Adv. Mater.* **2012**, *24*, 1176–1181.
- (30) Zhou, W.; Yu, Y.; Chen, H.; Disalvo, F. J.; Abruña, H. D. Yolk-Shell Structure of Polyaniline-Coated Sulfur for Lithium-Sulfur Batteries. *J. Am. Chem. Soc.* **2013**, *135*, 16736–16743.
- (31) Zhang, S.; Zhang, L.; Wang, W.; Xue, W. A Novel Cathode Material Based on Polyaniline Used for Lithium/Sulfur Secondary Battery. *Synth. Met.* **2010**, *160*, 2041–2044.
- (32) Meyer, B. Elemental Sulfur. *Chem. Rev.* **1976**, *76*, 367–388.
- (33) Yu, X.; Xie, J.; Yang, J.; Huang, H.; Wang, K.; Wen, Z. S. Lithium Storage in Conductive Sulfur-Containing Polymers. *J. Electroanal. Chem.* **2004**, *573*, 121–128.
- (34) Zhang, S. S. Understanding of Sulfurized Polyacrylonitrile for Superior Performance Lithium/Sulfur Battery. *Energies* **2014**, *7*, 4588–4600.
- (35) Ryu, H. S.; Guo, Z. P.; Ahn, H. J.; Cho, G. B.; Liu, H. K. Investigation of Discharge Reaction Mechanism of Lithium/Liquid Electrolyte/Sulfur Battery. *J. Power Sources* **2009**, *189*, 1179–1183.
- (36) Song, J. X.; Xu, T.; Gordin, M. L.; Zhu, P. Y.; Lv, D. P.; Jiang, Y.-B.; Chen, Y. S.; Duan, Y. H.; Wang, D. H. Nitrogen-Doped Mesoporous Carbon Promoted Chemical Adsorption of Sulfur and Fabrication of High-Areal-Capacity Sulfur Cathode with Exceptional Cycling Stability for Lithium-Sulfur Batteries. *Adv. Funct. Mater.* **2014**, *24*, 1243–1250.
- (37) Zhu, P. Y.; Song, J. X.; Lv, D. P.; Wang, D. H.; Jaye, C.; Fischer, D. A.; Wu, T. P.; Chen, Y. S. Mechanism of Enhanced Carbon Cathode Performance by Nitrogen Doping in Lithium-Sulfur Battery: An X-ray Absorption Spectroscopic Study. *J. Phys. Chem. C* **2014**, *118*, 7765–7771.
- (38) Xin, S.; Gu, L.; Zhao, N. H.; Yin, Y. X.; Zhou, L. J.; Guo, Y. G.; Wan, L. J. Smaller Sulfur Molecules Promise Better Lithium-Sulfur Batteries. *J. Am. Chem. Soc.* **2012**, *134*, 18510–18513.
- (39) Fanous, J.; Wegner, M.; Grimminger, J.; Andresen, A.; Buchmeiser, M. R. Structure-Related Electrochemistry of Sulfur-Poly(acrylonitrile) Composite Cathode Materials for Rechargeable Lithium Batteries. *Chem. Mater.* **2011**, *23*, 5024–5028.
- (40) Song, J.; Gordin, M. L.; Xu, T.; Chen, S.; Yu, Z.; Sohn, H.; Lu, J.; Ren, Y.; Duan, Y.; Wang, D. Strong Lithium Polysulfide Chemisorption on Electroactive Sites of Nitrogen-Doped Carbon Composites For High-Performance Lithium-Sulfur Battery Cathodes. *Angew. Chem., Int. Ed.* **2015**, *54*, 4325–4329.
- (41) Lee, S. W.; Yabuuchi, N.; Gallant, B. M.; Chen, S.; Kim, B.; Hammond, P. T.; Shao-Horn, Y. High-Power Lithium Batteries from Functionalized Carbon-Nanotube Electrodes. *Nat. Nanotechnol.* **2010**, *5*, 531–537.
- (42) Li, B.; Jiang, B.; Fauth, D. J.; Gray, M. L.; Pennline, H. W.; Richards, G. A. Innovative Nano-layered Solid Sorbents for CO₂ Capture. *Chem. Commun.* **2011**, *47*, 1719–1721.
- (43) Jiang, B.; Kish, V.; Fauth, D. J.; Gray, M. L.; Pennline, H. W.; Li, B. Performance of Amine-Multilayered Solid Sorbents for CO₂ Removal: Effect of Fabrication Variables. *Int. J. Greenhouse Gas Control* **2011**, *5*, 1170–1175.
- (44) Li, B.; Jiang, B.; Boyce, B. M.; Lindsey, B. A. Multilayer Polypeptide Nanoscale Coatings Incorporating IL-12 for the Prevention of Biomedical Device-Associated Infections. *Biomaterials* **2009**, *30*, 2552–2558.
- (45) Varahramyan, K.; Lvov, Y. Nanomanufacturing by Layer-by-Layer Assembly-From Nanoscale Coating to Device Applications. *Proc. Inst. Mech. Eng., Part N* **2006**, *220*, 29–37.